

---

# Concurrence of Symmetry Breaking and Nonlocality Phase Transitions in Diffusion Models

---

**Yifan F. Zhang**

Department of Electrical and Computer Engineering  
Princeton University  
Princeton, NJ 08544, USA  
yz4281@princeton.edu

**Fangjun Hu**

QuEra Computing Inc.  
1284 Soldiers Field Road, Boston, MA 02135, USA  
fhu@quera.com

**Guangkuo Liu**

JILA and Department of Physics  
University of Colorado Boulder  
Boulder, CO 80309, USA  
guangkuo.liu@colorado.edu

**Mert Okayay**

CTQM and Department of Physics  
University of Colorado Boulder  
Boulder, CO 80309, USA  
mert.okyay@colorado.edu

**Xun Gao**

JILA and Department of Physics  
University of Colorado Boulder  
Boulder, CO 80309, USA  
xun.gao@colorado.edu

## Abstract

Diffusion models undergo a phase transition in a critical time window during generation dynamics, with two complementary diagnoses of criticality. The symmetry breaking picture views the critical window as when trajectories bifurcate into different semantic minima of the energy landscape, whereas the nonlocality picture views the critical window as when local denoising fails. We study whether two notions of such phase transitions are concurrent in modern diffusion transformers. By evaluating the dynamics and outcomes of the generation trajectory, we observe a near-simultaneous occurrence of the non-locality and symmetry breaking critical times. Our work is the first to unify the two notions of phase transitions in practice: it provides a concrete diagnostic for when and why diffusion models rely on conditioning and global denoising, enabling principled evaluation of model efficiency and guiding the design of architectures and sampling schemes that avoid unnecessary computation.

**Code:** [https://github.com/zsxqblz/symmetry\\_nonlocality\\_transition](https://github.com/zsxqblz/symmetry_nonlocality_transition)

## 1 Introduction

Diffusion models now produce high-quality images, but we still have a limited understanding of *when* different capabilities turn on during generation. A diffusion trajectory is not a uniform process: the model does not use all signals equally at all times. One influential line of work borrows techniques from statistical mechanics and interprets the generation process as a *symmetry breaking*<sup>1</sup> phase

---

<sup>1</sup>Although “symmetry breaking” is a somewhat imprecise term—given that semantic minima are not necessarily symmetric—we adopt it because it is standard in the literature Raya and Ambrogioni [2023] and effectively conveys the underlying physical concept.

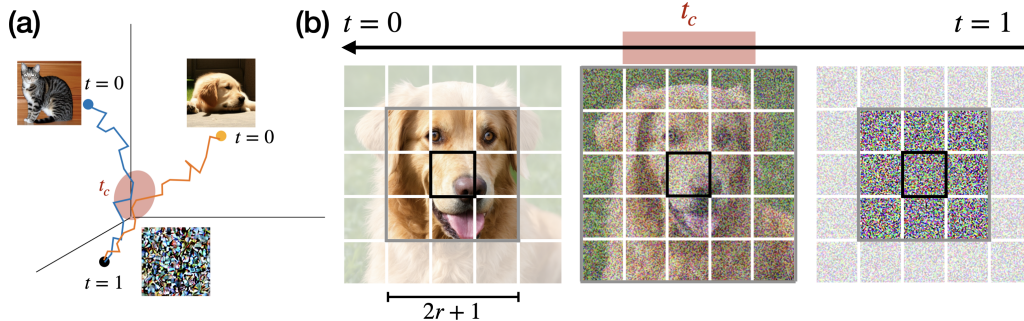


Figure 1: **Two definitions of phase transitions.** (a) Symmetry breaking phase transition. At  $t = 1$ , the energy landscape has one global minimum. As  $t$  approaches the phase transition, multiple local minima start to appear. (b) Nonlocality phase transition. Inside a phase, noise on a patch (black box) can be removed by using information in a small neighborhood (gray box). Near the phase transition, this neighborhood grows to be comparable to the entire image.

transition, where the distribution evolves from a single unstructured basin to multiple class- or prompt-consistent basins Raya and Ambrogioni [2023]. This picture predicts the existence of a “critical window” of time during which the dynamics has drastic impact on the output, such as changing the class or prompt semantics, while similar interventions outside that window have much smaller effects.

The statistical mechanics perspective is intuitive (and natural), as the diffusion model essentially mimics a non-equilibrium “cooling” from high-temperature Gaussian noise to low-temperature data distribution Sohl-Dickstein et al. [2015]. However, this symmetry breaking paradigm is ignorant of the spatial structure of the data. For example, the image distribution undergoes the same symmetry breaking transition regardless of whether the model treats the image as a vectorization of pixels or as a structured 2D array. Since locality bias is a key inductive bias in dataset Kamb and Ganguli [2024] and model design, it is important to understand how it interacts with the phase-transition picture.

Tools and concepts to tackle the connection between phase transitions and locality has recently been developed in the many-body physics and quantum error correction community: a complementary notion of criticality, a *nonlocality* phase transition, has been proposed Sang and Hsieh [2025]. This perspective puts locality front and center, and asks when local neighborhoods of a site contains enough information for denoising. At a higher noise rate, information is further corrupted, so the denoiser needs to look at a larger neighborhood to recover one patch. The noise level at which the denoising radius diverges is understood as a phase transition in which global information is needed to perform denoising, which may contain information such as the symmetry sector in which the initial condition was. In diffusion models, the identical information-theoretic probe has been found to gives rise to a critical window in which local denoising fails Hu et al. [2025]. This criticality may be inherently distinct from phase transitions in equilibrium statistical mechanics, e.g., because it is based on a purely operational criterion and does not follow from a free-energy argument.

This paper aims to reconcile these two notions in frontier models. Our starting hypothesis is simple: they should be related because semantics typically carry nonlocal information. If a model is actively injecting semantic identity (for example, deciding between a Golden Retriever dog and a golden British Shorthair cat, which can share similar local fur textures but differ in global shape and anatomy), it should also require long-range context. Conversely, if denoising can be done from local texture statistics alone, strong semantic guidance should be less necessary. In short, these arguments suggest that *symmetry breaking predicts when semantic forcing is needed, and nonlocality predicts when nonlocal computation is needed*; if semantics are globally organized, the two windows should align.

Figure 1 clarifies the two notions of phase-transitions. Panel (a) depicts the critical window for symmetry breaking: as diffusion proceeds, trajectories in high-dimensional state space branch into distinct semantic basins (for example, cat-like versus dog-like minima). Panel (b) depicts a locality transition for patch denoising: once global semantic identity is already stable, recovering a local region (such as a dog’s nose) may require only a small neighborhood (such as the head), whereas near a critical window where semantic identity is still unresolved or ambiguous, denoising must use broader, often global, context to inject the correct semantics.

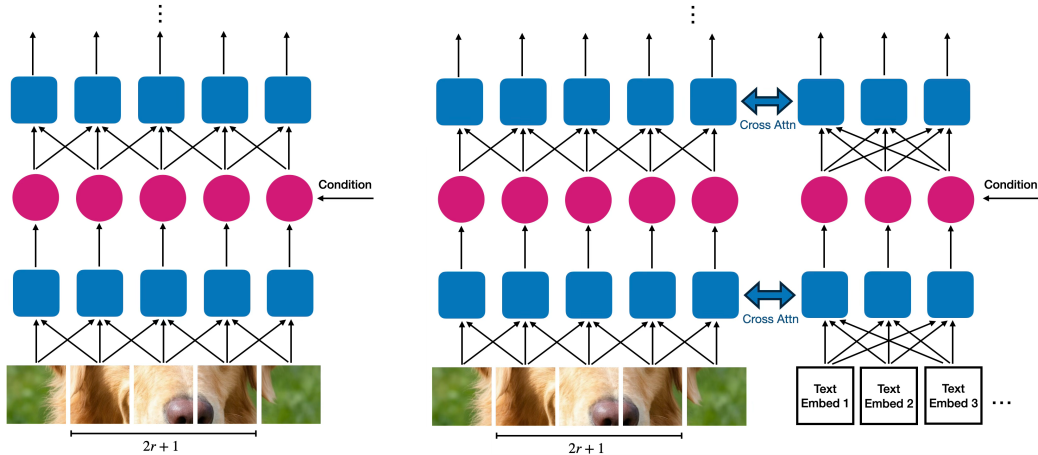


Figure 2: **DiT with local attention.** (a) In class-conditioned DiT, we restrict image-token attention to a local window with radius  $r$  and window size  $2r + 1$ . We visualize a one-dimensional strip of image tokens for simplicity. The conditioning signal still affects each token. (b) In multi-model DiT (MMDiT), we restrict image token-image token attention to a local window with radius  $r$ . Text token-text token and image token-text token attentions remain dense, so conditioning enters through both token-wise modules and cross attention.

## 1.1 Summary of Main Results

We probe the two definitions of critical window numerically from modern diffusion transformers (DiTs) and examine how they align. We use two complementary families of probes. The *instantaneous probe* directly measures score vectors along different trajectories. It compares conditional versus unconditional scores, and measures the symmetry breaking critical window where the difference is large. It also compares the global versus locally-approximated scores, and measures the nonlocality critical window where the difference is large. If the two critical windows are aligned, we conclude that the two phase transitions occur at the same time.

We complement the instantaneous probe with a series of *integrated probes*, which focus on how the dynamics influence the final generated samples. These probes include the standard forward-backward experiments Biroli et al. [2024], Li et al. [2025] used to define symmetry breaking critical times, as well as a series of sliding window methods where we switch between conditional and unconditional, global and local denoisers in a time window of the denoising process. We benchmark the quality of generation and ask when global or conditional denoising is necessary to complete the tasks with high quality.

We find concurrence of symmetry breaking and nonlocality in both probes. For instantaneous probes in the Facebook DiT-XL model Peebles and Xie [2023], the conditional versus unconditional gap becomes large in an early window centered near  $t \approx 0.2$ , and the local versus global gap is large in the same window. In Stable Diffusion 3 (SD3) Medium model Esser et al. [2024], both gaps concentrate very close to the noisy endpoint  $t = 1$ . The co-occurrence of the two gaps gives operational evidence that semantic forcing and nonlocal computation turn on together.

In integrated probes, we find concurrence as well. Facebook DiT-XL shows a critical window for both symmetry breaking and nonlocality near  $t \approx 0.5$ . This window is later than the window found in instantaneous probes, which can be interpreted as suboptimality: the model uses conditioning and non-local computation at an earlier  $t$  than when it is actually needed. In contrast, the higher-performance model, SD3 medium, shows a concurrent locality and symmetry breaking phase transition close to  $t = 1$  in both instantaneous probes and integrated probes.

## 2 Theoretical Background

### 2.1 Diffusion models and the score function

Let  $x_0 \sim p_{\text{data}}$  denote a clean data sample (e.g., an image in pixel or latent space), and let  $x_t$  denote its noised version at diffusion time  $t \in (0, 1]$  such that  $t = 1$  is the high-noise limit. The continuous-time Gaussian forward noising process can be written as an SDE

$$dx_t = f(x_t, t) dt + g(t) dW_t, \quad (1)$$

whose time-reversal admits the reverse-time SDE Ho et al. [2020]

$$dx_t = [f(x_t, t) - g^2(t) s^*(x_t, t)] dt + g(t) d\bar{W}_t, \quad (2)$$

where  $\bar{W}_t$  is a standard Brownian motion running backwards in time. The function  $s^*(x_t, t)$  is called the score at time  $t$ , and it is the gradient of the log density  $s^*(x_t, t) = \nabla_{x_t} \log q_t(x_t)$  where  $q_t$  is the marginal distribution of  $x_t$ . Diffusion models learn a parametric approximation  $s_\theta(x_t, t)$  to  $s^*(x_t, t)$  (or an equivalent parameterization) via denoising score matching Song et al. [2021]. The learned score  $s_\theta$  defines reverse-time dynamics that turns noise into a sample from the model distribution by initializing  $x_1 \sim \mathcal{N}(0, I)$  and numerically integrates the reverse SDE from  $t = 1$  to  $t = 0$ .

### 2.2 Symmetry breaking in sampling and classifier-free guidance

Its origin in statistical physics invites a study of diffusion dynamics, where early work noticed varying relative importance of different times Song et al. [2022], Choi et al. [2022], Raya and Ambrogioni [2023] for sample quality and class. These observations were studied in physics-inspired toy models Biroli and Mézard [2023], Ambrogioni [2025], motivating the terminology ‘symmetry-breaking’ for when the output sample is placed in a class during the diffusion path.

In many applications we want to sample the conditional distribution  $p_\theta(x | y)$  for a specified condition  $y$  (in addition to the marginal  $p_\theta(x)$ ), which requires access to the conditional score  $\nabla_{x_t} \log p_\theta(x_t | y)$  for all  $t$ . The modern approach to obtain a conditional sampler is known as classifier-free guidance (CFG) Ho and Salimans [2022], where the *same* parameters learn both a conditional score  $s_\theta(x_t, t | y)$  and an unconditional score  $s_\theta(x_t, t)$ . During sampling, CFG mixes the two scores to form a ‘guided score’

$$s_{\text{cfg}}(x_t, t | y) = s_\theta(x_t, t) + w(s_\theta(x_t, t | y) - s_\theta(x_t, t)), \quad (3)$$

where  $w \geq 0$  is the guidance scale. To make contact with physics, we write scores as gradients of energies  $U$  such that  $s = -\nabla U$ , and CFG can be viewed as sampling from an energy tilted by an external field:

$$U_{\text{cfg}}(x_t, t | y) = (1 - w)U_{\text{uncond}}(x_t, t) + w U_{\text{cond}}(x_t, t | y) + \text{const}. \quad (4)$$

Viewing each class as as a local minima of the conditional energy landscape  $U_{\text{cond}}(x_t, t | y)$ , the CFG weighted term plays the role of a bias that breaks the symmetry. The absence of a symmetry-breaking field implies that there needs to be spontaneous symmetry breaking for the model to pick a class, which has been associated with experimental failures of forward-backward experiments Ambrogioni [2026], Sclocchi et al. [2025b].

### 2.3 Local score function via approximate Markovianity

A separate line of work characterises phases of quantum distributions by local recoverability: between two distributions Sang and Hsieh [2025] proposed the decay length-scale of conditional mutual information (CMI) (the ‘Markov length’) to diagnose when one is not locally recoverable from the other. Bringing these insights to learning, Hu et al. [2026] has shown that if the CMI remains short-ranged during diffusion, then one can construct a sampler that outputs from this distribution using only local operations. On the other hand, Kumar et al. [2026] shows that distributions with long-ranged CMI is generically hard to learn.

We encode locality via a tripartition of the image  $X = (x_A, x_B, x_C)$  as shown in Figure 1 where  $A, B, C$  denote the innermost box, the surrounding annulus, and the rest, respectively. If the distribution  $p(x_A, x_B, x_C)$  forms a Markov chain, i.e.,  $p(x_A | x_B, x_C) = p(x_A | x_B)$ , then the score on region

$A$  depends only on  $(x_A, x_B)$  where  $\nabla_{x_A} \log p(x_A, x_B, x_C) = \nabla_{x_A} \log p(x_A | x_B)$  and the CMI would vanish. This property might hold approximately, which is quantified as rapidly-decaying CMI

$$I(A : C | B) \approx I_0 \exp(-d_{AC}/\xi), \quad (5)$$

where  $d_{AC}$  is a distance between regions  $A$  and  $C$ , and  $\xi$  is the Markov length. In such cases, we can find a good local approximation to the true score  $s_A(x_A, x_B, x_C)$ , where  $s_A^{\text{loc}}(x_A, x_B) = \nabla_{x_A} \log p(x_A | x_B)$ , which we expect to be accurate in real images. For example, to generate the nose of a dog, the model may only need to look at a neighborhood containing the snout and eyes, and not the rest of the image.

### 3 Experiments

We study two diffusion transformer systems: a Facebook DiT-XL class-conditional ImageNet model and SD3 medium, a text-conditioned MMDiT model. As before, throughout the experiments,  $t = 1$  denotes the noisy endpoint and  $t = 0$  denotes the clean endpoint.

#### 3.1 Constructing local denoisers

Training a local denoiser could be computationally expensive. Instead, we take any pre-trained DiT and construct a local version of it, which also has the benefit of understanding model’s internal circuitry. For each image token, we truncate the attention window to a small radius  $r$  around itself as shown in Figure 2(a). Note that for Facebook DiT-XL, class and time conditioning is injected into each patch independently through AdaLN Perez et al. [2018], Peebles and Xie [2023]. Since the conditioning is still computed globally, in principle the model is capable of providing global conditioning information to each patch even when image-token attention is local. For MMDiT model such as SD3, both image and text tokens enter the joint attention. Therefore, we only restrict image token–image token attention to a local window, while keeping text token–text token and image token–text token attentions dense, as described in Figure 2(b). This way, the conditioning signal can still be globally available to each patch through both cross attention and text token self attention.

We also note that the truncation procedure does not produce a strictly local denoiser, as context from patches further than  $r$  can still enter by propagating through multiple local attention steps. One should therefore view the truncated DiT as an approximation with strong locality bias rather than a strictly local denoiser. This is in fact operationally meaningful, since we are performing a minimal perturbation to the original model architecture, which in principle saves a large amount of compute.

#### 3.2 Instantaneous probe: score gap

We first probe the phase transition through the instantaneous probe, which measures the behavior of the score function along the sampling and training trajectories. We take the conditional score function  $s_\theta(x_t, t | y)$  and the unconditional score function  $s_\theta(x_t, t)$ , define the *conditioning gap* as the  $l_2$  norm of their difference:

$$\Delta \vec{s}_{\text{cond}}(x_t, t | y) = s_\theta(x_t, t) - s_\theta(x_t, t | y), \quad (6)$$

The conditioning gap provides a direct, model-internal readout of how strongly the condition changes the denoising vector at time  $t$ .

For nonlocality, we construct local denoiser from pretrained model following Figure 2 which provides a local score function  $s_{\theta,r}(x_t, t)$  from the global score function  $s_\theta(x_t, t)$ . The *locality gap* is then defined as the  $l_2$  norm of their difference.

The truncated DiT gives a local approximation of the score function  $s_{\text{local},r}(x_t, t)$ . to the original global score function  $s_{\text{global}}(x_t, t)$ . We define the locality gap

$$\Delta \vec{s}_{\text{loc}}(x_t, t, r) = s_\theta(x_t, t) - s_{\theta,r}(x_t, t). \quad (7)$$

The above definition is valid for both conditional and unconditional score function. If the trained model can compute the relevant score locally at time  $t$ , this gap should be small for modest  $r$ . If global information is necessary, the gap should remain large until  $r$  is sufficiently large. This gives a direct operational version of the CMI-based nonlocality probe. Throughout this paper, we sample

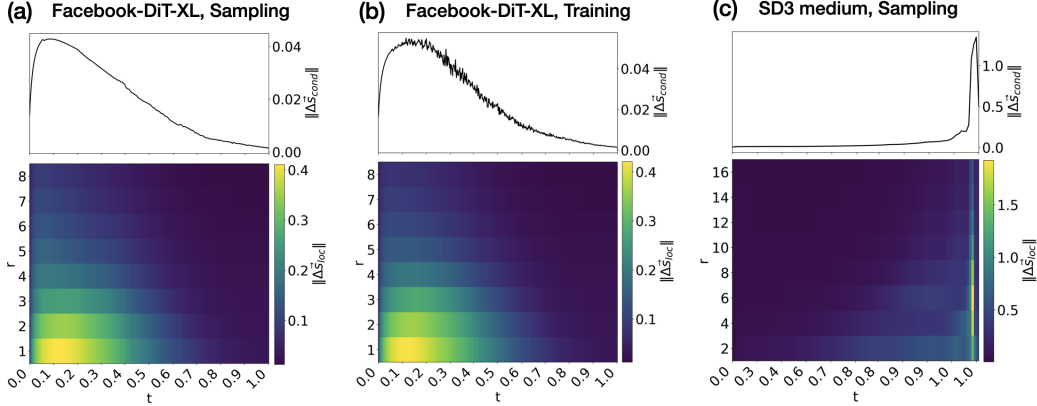


Figure 3: **Conditioning gap vs. locality gap.** Top row: the one-dimensional plot shows the conditioning gap  $\|\Delta\vec{s}_{\text{cond}}\|$  as a function of  $t$ . Bottom row: the heatmap shows the locality gap  $\|\Delta\vec{s}_{\text{loc}}\|$ , defined using conditional score function, as a function of attention radius  $r$  and time  $t$ . (a) Facebook DiT-XL along the sampling trajectory. (b) Facebook DiT-XL along the training trajectory. (c) SD3 medium along the sampling trajectory; the horizontal axis is reversed so that sampling proceeds left to right. In all three panels, the two gaps align remarkably well despite being functionally independent probes.

images of  $256 \times 256$  pixels for Facebook DiT and  $512 \times 512$  pixels for SD3 medium. Both models we consider have patch size of 16 pixels, so in our study, setting  $r = 16$  for Facebook DiT /  $r = 32$  for SD3 medium reduces local denoiser to global denoiser.

We first ask whether the two score gaps identify the same time window. Figure 3 plots the conditioning gap on the top row and the locality gap on the bottom row. We normalize the gap by the number of image tokens. The top row measures the strength of the semantic field induced by conditioning. The bottom row measures the cost of replacing the global denoiser with a local one: large values indicate that the model’s score cannot be reproduced from local image context alone.

For Facebook DiT-XL, Figure 3(a,b), the conditioning gap is initially small at  $t$  close to zero. This is intuitive, as the semantics are still present in slightly noisy images, so conditioning is unnecessary. As  $t$  increases, it become large at saturate near  $t \approx 0.2$ . They it decays as the trajectory approaches the clean endpoint. This behavior is consistent with the phenomenology of symmetry breaking phase transition, and is also consistent with the empirical observation of when conditioning is beneficial Kynkäänniemi et al. [2024], Jin et al. [2025].

The behavior of the locality gap is largely aligned with the conditioning gap. at early and late time, locality gap quickly decays at increasing  $r$ , indicating that local denoisers approximate global denoiser well. Around  $t \approx 0.2$ , locality gap remains large even at large  $r$ . The behaviors are similar between training and sampling trajectories, indicating a good generalization of the model.

For SD3 medium, Figure 3(c,d), the behavior of both gaps are large the same and are aligned. We also observe a richer behavior when sending different prompts. For example, when prompting for violin (Figure 3(d)), we observe two peaks in conditioning and locality gaps near  $t = 1$ . We also observe a weaker peak at a lower  $t$ .

The conditioning and locality gaps are independent quantities: one compares conditional and unconditional scores, while the other compares global and local computation under the same conditioning setup. Their alignment therefore gives direct evidence that the symmetry breaking transition and the nonlocality transition are linked. The locality-gap heatmaps play the same role operationally that CMI heatmaps play in Hu et al. [2025]: both identify times when distant context is needed, but our probe uses an actual truncated denoiser rather than an information-theoretic decoder.

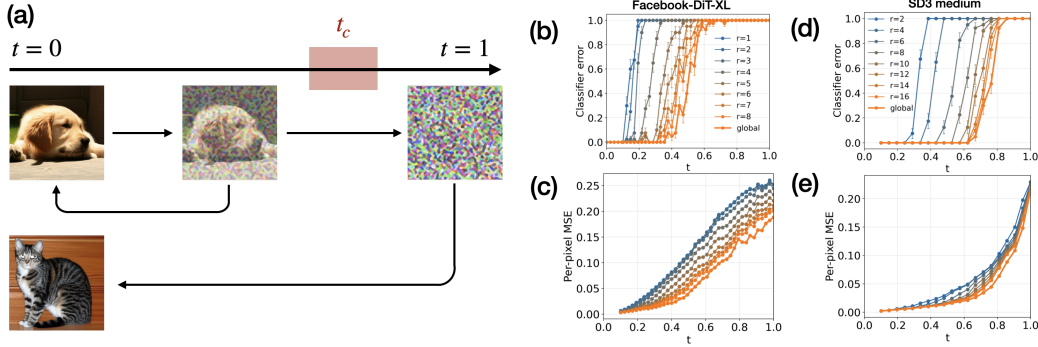


Figure 4: **Forward-backward experiment.** (a) Schematic of the error-correction experiment. When the noise level is below a threshold, the unconditional denoiser recovers the same class; when the noise level is above the threshold, the unconditional denoiser can recover a different class. (b,d) Classification error of images denoised from different noise levels  $t$  for Facebook DiT-XL and SD3 medium. Curves labeled by  $r$  use local denoisers with attention radius  $r$  (see Fig 2); the global curve uses the original denoiser. (c,e) Per-pixel MSE of the denoised image relative to the clean image.

### 3.3 Integrated probe: forward-backward error correction

The model-internal details captured by gaps (6) and (7) may be smeared out during sampling (which integrates over time), so we need integrated probes which directly benchmark the downstream samples. The first is the ‘forward-backwards experiment’ illustrated in Figure 4(a): start from a clean image, add noise forward to time  $t$ , and then denoise backward unconditionally. If the noised state remains inside the basin of the original semantic class, the unconditional denoiser recovers an image from the same class. If  $t$  crosses the semantic error threshold, the unconditional denoiser can return an image from a different class. This is also a standard probe of symmetry breaking phase transition in early studies by Biroli et al. [2024], Sclocchi et al. [2025c], Li et al. [2025].

Figures 4(b,d) plot the classifier-error rate of the denoised image using Facebook DiT-XL and SD3 medium. Both models show sharp classifier-error jumps as  $t$  increases. For Facebook DiT-XL, Figure 4(b), the global threshold is around  $t \approx 0.5$ . Local denoisers also exhibit sharp thresholds, and those thresholds move toward the global threshold as  $r$  increases. This indicates that local denoising has its own error-correction transition, and that larger local neighborhoods recover more of the global denoiser’s semantic capability.

For SD3 medium, Figure 4(d), the corresponding threshold is very close to  $t = 1$ , and local thresholds again approach the global threshold as  $r$  grows. It is expected that SD3 medium has a larger threshold: it is more powerful and therefore should be a better decoder. This leads to the following prediction: stronger models have critical window at larger  $t$ . We leave the validation of this prediction to future work.

Figures 4(c,e) show a complementary low-level metric. The per-pixel MSE increases smoothly and sublinearly with  $t$ , with an almost flat derivative at small  $t$ . This is consistent with error correction: small forward noise can be removed without large reconstruction error. However, MSE does not expose the semantic transition. The semantic class can be destroyed abruptly while the pixelwise error curve remains smooth, because semantic information is nonlocal and is not visible in a per-pixel distortion measure.

This experiment also separates two kinds of alignment. Within the forward-backward probe, the global and local denoisers both show sharp thresholds, and the local thresholds converge toward the global threshold with larger radius. Across probes, however, Facebook DiT-XL is misaligned: the instantaneous score-gap window is near  $t \approx 0.2$ , while the integrated semantic error threshold is near  $t \approx 0.5$ . We interpret this as evidence that Facebook DiT-XL performs unnecessary conditioning and nonlocal computation at low  $t$ . SD3 medium is more aligned across probes, with close to  $t = 1$  transitions predicted by both instantaneous and integrated probes.

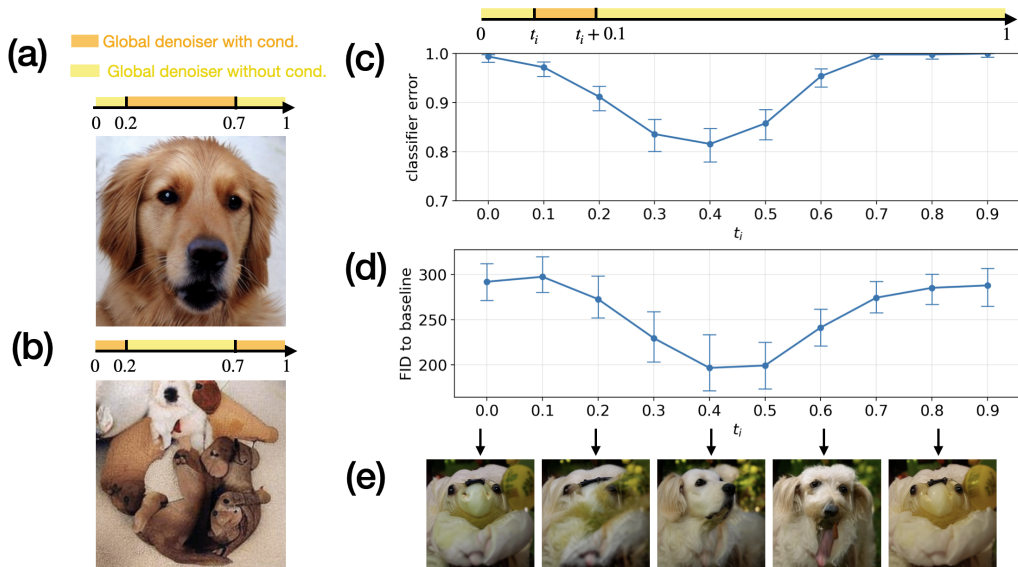


Figure 5: **Time-windowed conditioning in Facebook DiT-XL.** Left column: (a) Golden retriever sample generated with conditioning applied only in the time window  $[0.2, 0.7]$  and no conditioning outside the window. (b) Sample generated with conditioning removed in  $[0.2, 0.7]$  and applied outside the window. Right column: samples generated with conditioning applied only in short windows  $[t_i, t_i + 0.1]$  while scanning  $t_i$ . (c) Classification error as a function of  $t_i$ . (d) FID to always-conditioned samples as a function of  $t_i$ . (e) Visualization of generated samples at different  $t_i$ .

### 3.4 Integrated probe: windowed conditioning

We next ask when conditioning is necessary for actual sampling. The symmetry breaking picture predicts that conditioning is most important near the critical window. We first demonstrate this idea with Facebook DiT-XL in Figure 5. Results for SD3 medium are in the appendix. Figure 5(a) shows that applying conditioning only during  $[0.2, 0.7]$ , which covers the critical window predicted from forward-backward experiment, can produce a recognizable golden retriever. Figure 5(b) shows the complementary intervention: applying conditioning outside  $[0.2, 0.7]$  but removing it inside the window produces a much worse semantic result. Thus the outside-window conditioning is not enough, even though local textures and image statistics may still look plausible.

To quantitatively pin down the critical window, we choose a short interval  $[t_i, t_i + 0.1]$  for conditioning and scan over  $t_i$ . We expect that when  $[t_i, t_i + 0.1]$  overlaps with the critical window the most, the sample has better quality. Figure 5(c) shows that classifier error is lowest around  $t_i \approx 0.4$ , and Figure 5(d) shows that Fréchet inception distance (FID) to the always-conditioned baseline is also lowest around the same time. The samples in Figure 5(e) visualize this dependence: semantic correctness emerges when conditioning is placed in the critical window. This indicates an alignment with the forward-backward experiment. The SD3 medium windowed-conditioning experiment is shown in the appendix (Figure 7) and exhibits similar alignment.

We also note that the classifier error and FID are overall large. This is because we heavily corrupt the model and sampling dynamics. The argument is not to have a small classifier error / FID overall, but to test which  $t_i$  corrupts these benchmarks minimally.

### 3.5 Integrated probe: windowed local/global denoising

The windowed-conditioning experiments test when semantic conditioning is needed. We now test when global denoising is needed. In these experiments, a global denoiser is used inside a time window and a local denoiser is used outside it, or vice versa.

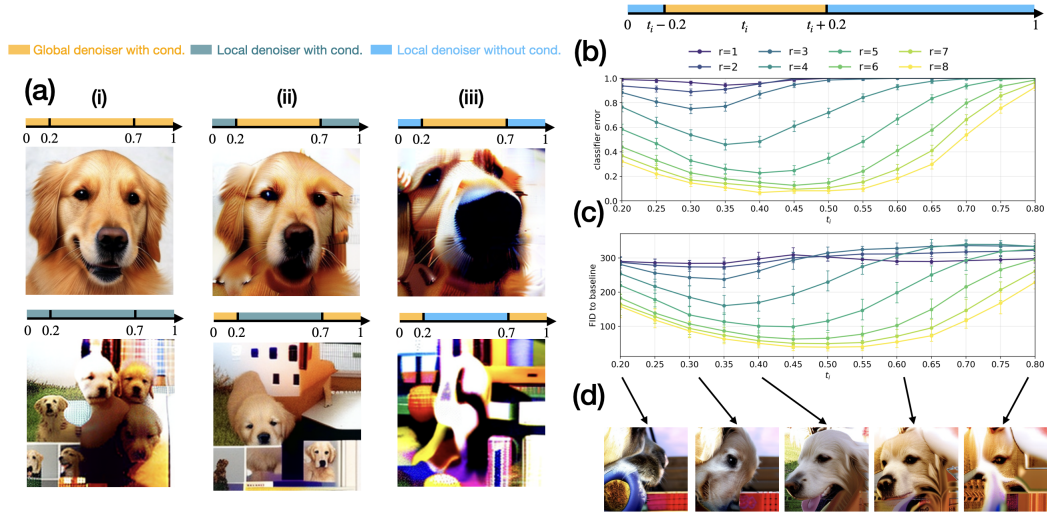


Figure 6: **Time-windowed local denoising in Facebook DiT-XL.** (a) Golden retriever samples generated with different combinations of local and global denoisers. The local denoiser uses radius  $r = 3$ . (i) Top: global denoiser at all times. Bottom: local denoiser at all times. (ii) Top: global denoiser in  $[0.2, 0.7]$  and local conditioned denoiser outside the window. Bottom: local conditioned denoiser in  $[0.2, 0.7]$  and global denoiser outside the window. (iii) Top: global denoiser in  $[0.2, 0.7]$  and local unconditional denoiser outside the window. Bottom: local unconditional denoiser in  $[0.2, 0.7]$  and global denoiser outside the window. Right column: samples generated with a global denoiser in  $[t_i - 0.2, t_i + 0.2]$  and a local unconditional denoiser with different  $r$  outside the window while scanning  $t_i$ . (b) Classification error as a function of  $t_i$ . (c) FID to always-global samples as a function of  $t_i$ . (d) Visualization of generated samples at different  $t_i$  using  $r = 3$ .

We start with visual examples using Facebook DiT-XL (SD3 medium in Appendix). Figure 6(a)(i) compares the two extremes: an always-global denoiser produces a clean golden retriever, while an always-local denoiser gives “domains” of small dogs (with size comparable to  $r$ ) smoothly merged together. This can be understood as the creative samples from Kamb and Ganguli [2024]. Figure 6(a)(ii) shows that using the global denoiser during  $[0.2, 0.7]$  and a local conditioned denoiser outside that window preserves a globally coherent dog better than the reverse schedule. Figure 6(a)(iii) makes the separation from conditioning sharper: even when the outside-window local denoiser is unconditional, putting global denoising in the critical window remains helpful, whereas replacing the critical window by local denoising is much worse.

To pin down the critical window for nonlocality phase transition, we scan a global conditioning window  $[t_i - 0.2, t_i + 0.2]$  and use local unconditional denoiser outside. Figures 6(b,c) show that classifier error and FID are again minimized when the global-denoising window is centered near  $t_i \approx 0.4$ . The samples in Figure 6(d) visualize the same window dependence. We also observe a slight increase in the minima at increasing  $r$ . We hypothesize that this is related to the increasing threshold at increasing  $r$  in the forward-backward experiment (Figure 4). At a fixed  $r$  the observed critical window is earlier than the actual critical window, but the difference vanishes at increasing  $r$ . Together with previous integrated probe results, we establish an alignment between symmetry breaking and nonlocality transition, through error correction and sampling.

## 4 Conclusion

Our work provides a unified operational view of two notions of phase transitions in diffusion models. By connecting symmetry breaking induced by conditioning with the onset of nonlocal computation in the score, we show that both phenomena can be detected through the same set of measurable quantities. This yields a concrete diagnostic for identifying when global communication is actually required during sampling, rather than assumed a priori from model design. In particular, the agreement (or

mismatch) between instantaneous score-based probes and integrated sampling behavior directly reveals how efficiently a model uses its conditioning signal and attention mechanism over time.

These observations have direct implications for both model design and training. On the architecture side, they motivate designs that explicitly control when and how global communication is enabled—for example, by gating cross-token attention, restricting receptive fields outside the critical window, or structuring conditioning pathways so that symmetry breaking is delayed until it is needed. On the training side, the phase diagram suggests reweighting losses or noise schedules to concentrate learning signal near the critical interval, encouraging the model to align symmetry breaking with the onset of nonlocality. One can also regularize locality (e.g., via masked attention or locality constraints) at early times and gradually relax these constraints during training, effectively shaping the trajectory of the learned score.

More broadly, our framework suggests a principled route to improving diffusion models. It enables systematic comparison across architectures by reducing complex generation behavior to phase diagrams over time, and it supports adaptive sampling schemes that switch between local and global denoisers based on the identified critical window. It also provides concrete guidance for co-designing architectures and training procedures so that useful global computation is both temporally localized and computationally efficient, opening the possibility of achieving comparable or improved generation quality with significantly reduced cost.

## References

- Luca Ambrogioni. The statistical thermodynamics of generative diffusion models: Phase transitions, symmetry breaking, and critical instability. *Entropy*, 27(3), 2025. ISSN 1099-4300. doi: 10.3390/e27030291. URL <https://www.mdpi.com/1099-4300/27/3/291>.
- Luca Ambrogioni. How out-of-equilibrium phase transitions can seed pattern formation in trained diffusion models, 2026. URL <https://arxiv.org/abs/2603.20092>.
- Giulio Biroli and Marc Mézard. Generative diffusion in very large dimensions. *Journal of Statistical Mechanics: Theory and Experiment*, 2023(9):093402, September 2023. ISSN 1742-5468. doi: 10.1088/1742-5468/acf8ba. URL <http://dx.doi.org/10.1088/1742-5468/acf8ba>.
- Giulio Biroli, Tony Bonnaire, Valentin de Bortoli, and Marc Mézard. Dynamical regimes of diffusion models. *Nature Communications*, 15(1):9957, November 2024. ISSN 2041-1723. doi: 10.1038/s41467-024-54281-3. URL <https://doi.org/10.1038/s41467-024-54281-3>.
- Jooyoung Choi, Jungbeom Lee, Chaehun Shin, Sungwon Kim, Hyunwoo Kim, and Sungroh Yoon. Perception prioritized training of diffusion models. In *2022 IEEE/CVF Conference on Computer Vision and Pattern Recognition (CVPR)*, pages 11462–11471, 2022. doi: 10.1109/CVPR52688.2022.01118.
- Jia Deng, Wei Dong, Richard Socher, Li-Jia Li, Kai Li, and Li Fei-Fei. Imagenet: A large-scale hierarchical image database. In *2009 IEEE conference on computer vision and pattern recognition*, pages 248–255. Ieee, 2009.
- Patrick Esser, Sumith Kulal, Andreas Blattmann, Rahim Entezari, Jonas Müller, Harry Saini, Yam Levi, Dominik Lorenz, Axel Sauer, Frederic Boesel, Dustin Podell, Tim Dockhorn, Zion English, Kyle Lacey, Alex Goodwin, Yannik Marek, and Robin Rombach. Scaling rectified flow transformers for high-resolution image synthesis, 2024. URL <https://arxiv.org/abs/2403.03206>.
- Yiqiu Han, Xiaoyang Huang, Zohar Komargodski, Andrew Lucas, and Fedor K Popov. Entropic order. *Nature Communications*, 2025.
- Florian Handke, Félix Koulischer, Gabriel Raya, and Luca Ambrogioni. Measuring semantic information production in generative diffusion models, 2025. URL <https://arxiv.org/abs/2506.10433>.
- Florian Handke, Dejan Stančević, Felix Koulischer, Thomas Demeester, and Luca Ambrogioni. The entropic signature of class speciation in diffusion models, 2026. URL <https://arxiv.org/abs/2602.09651>.

- Ali Hassani. Neighborhood attention: Dynamic restriction of self attention. Technical Report AREA-202307, University of Oregon, Department of Computer Science, 2023. URL <https://www.cs.uoregon.edu/Reports/AREA-202307-Hassani.pdf>.
- Ali Hassani and Humphrey Shi. Dilated neighborhood attention transformer, 2022. URL <https://arxiv.org/abs/2209.15001>.
- Ali Hassani, Steven Walton, Jiachen Li, Shen Li, and Humphrey Shi. Neighborhood attention transformer. In *Proceedings of the IEEE/CVF Conference on Computer Vision and Pattern Recognition (CVPR)*, pages 6185–6194, 2023. doi: 10.1109/CVPR52729.2023.00599.
- Kaiming He, Xiangyu Zhang, Shaoqing Ren, and Jian Sun. Deep residual learning for image recognition. In *Proceedings of the IEEE conference on computer vision and pattern recognition*, pages 770–778, 2016.
- Martin Heusel, Hubert Ramsauer, Thomas Unterthiner, Bernhard Nessler, and Sepp Hochreiter. Gans trained by a two time-scale update rule converge to a local nash equilibrium. *Advances in neural information processing systems*, 30, 2017.
- Jonathan Ho and Tim Salimans. Classifier-free diffusion guidance. *arXiv preprint arXiv:2207.12598*, 2022.
- Jonathan Ho, Ajay Jain, and Pieter Abbeel. Denoising diffusion probabilistic models. In *Proceedings of the 34th International Conference on Neural Information Processing Systems, NIPS '20*, Red Hook, NY, USA, 2020. Curran Associates Inc. ISBN 9781713829546.
- Fangjun Hu, Guangkuo Liu, Yifan F. Zhang, and Xun Gao. Local diffusion models and phases of data distributions, 2025. URL <https://arxiv.org/abs/2508.06614>.
- Fangjun Hu, Christian Kokail, Milan Kornjača, Pedro L. S. Lopes, Weiyuan Gong, Sheng-Tao Wang, Xun Gao, and Stefan Ostermann. Learning and generating mixed states prepared by shallow channel circuits. *arXiv:2604.01197 [quant-ph]*, 2026. URL <https://arxiv.org/abs/2604.01197>.
- Hugging Face and Microsoft. Resnet-50 v1.5. <https://huggingface.co/microsoft/resnet-50>, 2025.
- Cheng Jin, Qitan Shi, and Yuantao Gu. Stage-wise dynamics of classifier-free guidance in diffusion models. *arXiv preprint arXiv:2509.22007*, 2025.
- Mason Kamb and Surya Ganguli. An analytic theory of creativity in convolutional diffusion models. *arXiv preprint arXiv:2412.20292*, 2024.
- Tarun Advait Kumar, Yijian Zou, Amir-Reza Negari, Roger G. Melko, and Timothy H. Hsieh. Unlearnable phases of matter. *arXiv:2602.11262 [cond-mat.dis-nn]*, 2026. URL <https://arxiv.org/abs/2602.11262>.
- Tuomas Kynkäänniemi, Miika Aittala, Tero Karras, Samuli Laine, Timo Aila, and Jaakko Lehtinen. Applying guidance in a limited interval improves sample and distribution quality in diffusion models. In *Advances in Neural Information Processing Systems*, volume 37, 2024. DOI: 10.52202/079017-3892.
- Marvin Li and Sitan Chen. Critical windows: non-asymptotic theory for feature emergence in diffusion models. In *Proceedings of the 41st International Conference on Machine Learning, ICML'24*. JMLR.org, 2024.
- Marvin Li, Aayush Karan, and Sitan Chen. Blink of an eye: a simple theory for feature localization in generative models. In *Forty-second International Conference on Machine Learning*, 2025. URL <https://openreview.net/forum?id=QvqnPVGWAN>.
- Ze Liu, Yutong Lin, Yue Cao, Han Hu, Yixuan Wei, Zheng Zhang, Stephen Lin, and Baining Guo. Swin transformer: Hierarchical vision transformer using shifted windows. In *Proceedings of the IEEE/CVF International Conference on Computer Vision (ICCV)*, pages 10012–10022, 2021.

- Cheng Lu, Yuhao Zhou, Fan Bao, Jianfei Chen, Chongxuan Li, and Jun Zhu. Dpm-solver: A fast ode solver for diffusion probabilistic model sampling in around 10 steps. *Advances in neural information processing systems*, 35:5775–5787, 2022.
- Cheng Lu, Yuhao Zhou, Fan Bao, Jianfei Chen, Chongxuan Li, and Jun Zhu. Dpm-solver++: Fast solver for guided sampling of diffusion probabilistic models. *Machine Intelligence Research*, 22(4):730–751, 2025.
- Haiqi Lu and Ying Tang. Steering dynamical regimes of diffusion models by breaking detailed balance, 2026. URL <https://arxiv.org/abs/2602.15914>.
- Artem Lukoianov, Chenyang Yuan, Justin Solomon, and Vincent Sitzmann. Locality in image diffusion models emerges from data statistics. *arXiv preprint arXiv:2509.09672*, 2025.
- Chenlin Meng, Yutong He, Yang Song, Jiaming Song, Jiajun Wu, Jun-Yan Zhu, and Stefano Ermon. SDEdit: Guided image synthesis and editing with stochastic differential equations. In *International Conference on Learning Representations*, 2022. URL [https://openreview.net/forum?id=aBsCjcPu\\_tE](https://openreview.net/forum?id=aBsCjcPu_tE).
- N. D. Mermin and H. Wagner. Absence of ferromagnetism or antiferromagnetism in one- or two-dimensional isotropic heisenberg models. *Phys. Rev. Lett.*, 17:1133–1136, Nov 1966. doi: 10.1103/PhysRevLett.17.1133. URL <https://link.aps.org/doi/10.1103/PhysRevLett.17.1133>.
- Matthew Niedoba, Berend Zwartsenberg, Kevin Murphy, and Frank Wood. Towards a mechanistic explanation of diffusion model generalization. *arXiv preprint arXiv:2411.19339*, 2024.
- William Peebles and Saining Xie. Scalable diffusion models with transformers. In *Proceedings of the IEEE/CVF international conference on computer vision*, pages 4195–4205, 2023.
- Ethan Perez, Florian Strub, Harm De Vries, Vincent Dumoulin, and Aaron Courville. Film: Visual reasoning with a general conditioning layer. In *Proceedings of the AAAI conference on artificial intelligence*, volume 32, 2018.
- Bao Pham, Gabriel Raya, Matteo Negri, Mohammed J Zaki, Luca Ambrogioni, and Dmitry Krotov. Memorization to generalization: The emergence of diffusion models from associative memory. In *NeurIPS 2024 Workshop on Scientific Methods for Understanding Deep Learning*, 2024. URL <https://openreview.net/forum?id=zVMMaVy2BY>.
- Sai Niranjan Ramachandran, Manish Krishan Lal, and Suvrit Sra. Cross-fluctuation phase transitions reveal sampling dynamics in diffusion models. In *The Thirty-ninth Annual Conference on Neural Information Processing Systems*, 2026. URL <https://openreview.net/forum?id=b4X6cz1F9L>.
- Gabriel Raya and Luca Ambrogioni. Spontaneous symmetry breaking in generative diffusion models. In *Thirty-seventh Conference on Neural Information Processing Systems*, 2023. URL <https://openreview.net/forum?id=1xGFGMMSV1>.
- Shengqi Sang and Timothy H. Hsieh. Stability of mixed-state quantum phases via finite markov length. *Phys. Rev. Lett.*, 134:070403, Feb 2025. doi: 10.1103/PhysRevLett.134.070403. URL <https://link.aps.org/doi/10.1103/PhysRevLett.134.070403>.
- Antonio Sclocchi, Alessandro Favero, Noam Itzhak Levi, and Matthieu Wyart. Probing the latent hierarchical structure of data via diffusion models. In *Proceedings of the International Conference on Learning Representations (ICLR)*, 2025a. URL <https://arxiv.org/abs/2410.13770>.
- Antonio Sclocchi, Alessandro Favero, and Matthieu Wyart. A phase transition in diffusion models reveals the hierarchical nature of data. *Proceedings of the National Academy of Sciences*, 122(1):e2408799121, 2025b. doi: 10.1073/pnas.2408799121. URL <https://www.pnas.org/doi/abs/10.1073/pnas.2408799121>.
- Antonio Sclocchi, Alessandro Favero, and Matthieu Wyart. A phase transition in diffusion models reveals the hierarchical nature of data. *Proceedings of the National Academy of Sciences*, 122(1):e2408799121, 2025c. doi: 10.1073/pnas.2408799121.

- Kulin Shah, Alkis Kalavasis, Adam R. Klivans, and Giannis Daras. Does generation require memorization? creative diffusion models using ambient diffusion. *arXiv preprint arXiv:2502.21278*, 2025.
- Jascha Sohl-Dickstein, Eric Weiss, Niru Maheswaranathan, and Surya Ganguli. Deep unsupervised learning using nonequilibrium thermodynamics. In Francis Bach and David Blei, editors, *Proceedings of the 32nd International Conference on Machine Learning*, volume 37 of *Proceedings of Machine Learning Research*, pages 2256–2265, Lille, France, 07–09 Jul 2015. PMLR. URL <https://proceedings.mlr.press/v37/sohl-dickstein15.html>.
- Jiaming Song, Chenlin Meng, and Stefano Ermon. Denoising diffusion implicit models, 2022. URL <https://arxiv.org/abs/2010.02502>.
- Yang Song, Jascha Sohl-Dickstein, Diederik P Kingma, Abhishek Kumar, Stefano Ermon, and Ben Poole. Score-based generative modeling through stochastic differential equations. In *International Conference on Learning Representations*, 2021. URL <https://openreview.net/forum?id=PxTIG12RRHS>.
- Dejan Stančević and Luca Ambrogioni. The information dynamics of generative diffusion. *Entropy*, 28(2), 2026. ISSN 1099-4300. doi: 10.3390/e28020195. URL <https://www.mdpi.com/1099-4300/28/2/195>.
- Christian Szegedy, Vincent Vanhoucke, Sergey Ioffe, Jon Shlens, and Zbigniew Wojna. Rethinking the inception architecture for computer vision. In *Proceedings of the IEEE conference on computer vision and pattern recognition*, pages 2818–2826, 2016.
- Tomoei Takahashi, Takashi Takahashi, and Yoshiyuki Kabashima. Dynamical regimes of discrete diffusion models, 2026. URL <https://arxiv.org/abs/2604.10961>.
- Enrico Ventura, Beatrice Achilli, Luca Ambrogioni, and Carlo Lucibello. Emergence of distortions in high-dimensional guided diffusion models, 2026. URL <https://arxiv.org/abs/2602.00716>.
- Jiafu Wu, Yabiao Wang, Jian Li, Jinlong Peng, Yun Cao, Chengjie Wang, and Jiangning Zhang. Swindit: Diffusion transformer using pseudo shifted windows. *arXiv preprint arXiv:2505.13219*, 2025.
- Manato Yaguchi, Kotaro Sakamoto, Ryosuke Sakamoto, Masato Tanabe, Masatomo Akagawa, Yusuke Hayashi, Masahiro Suzuki, and Yutaka Matsuo. The geometry of phase transitions in diffusion models: Tubular neighbourhoods and singularities. *Transactions on Machine Learning Research*, 2025. ISSN 2835-8856. URL <https://openreview.net/forum?id=ahVFKFLYk2>. Featured Certification.
- Jinmin Yi, Kangle Li, Chuan Liu, Zixuan Li, and Liujun Zou. Universal decay of mutual information and conditional mutual information in gapped pure- and mixed-state quantum matter. *Phys. Rev. Lett.*, 136:116604, Mar 2026. doi: 10.1103/mqp8-y1m7. URL <https://link.aps.org/doi/10.1103/mqp8-y1m7>.
- Zhihang Yuan, Hanling Zhang, Pu Lu, Xuefei Ning, Linfeng Zhang, Tianchen Zhao, Shengen Yan, Guohao Dai, and Yu Wang. Ditfastattn: Attention compression for diffusion transformer models. In *Advances in Neural Information Processing Systems*, volume 37, 2024. DOI: 10.52202/079017-0037.
- Yifan Zhang and Sarang Gopalakrishnan. Conditional mutual information and information-theoretic phases of decohered gibbs states, 2025a. URL <https://arxiv.org/abs/2502.13210>.
- Yifan F. Zhang and Sarang Gopalakrishnan. Stability of mixed-state phases under weak decoherence, 2025b. URL <https://arxiv.org/abs/2511.01976>.

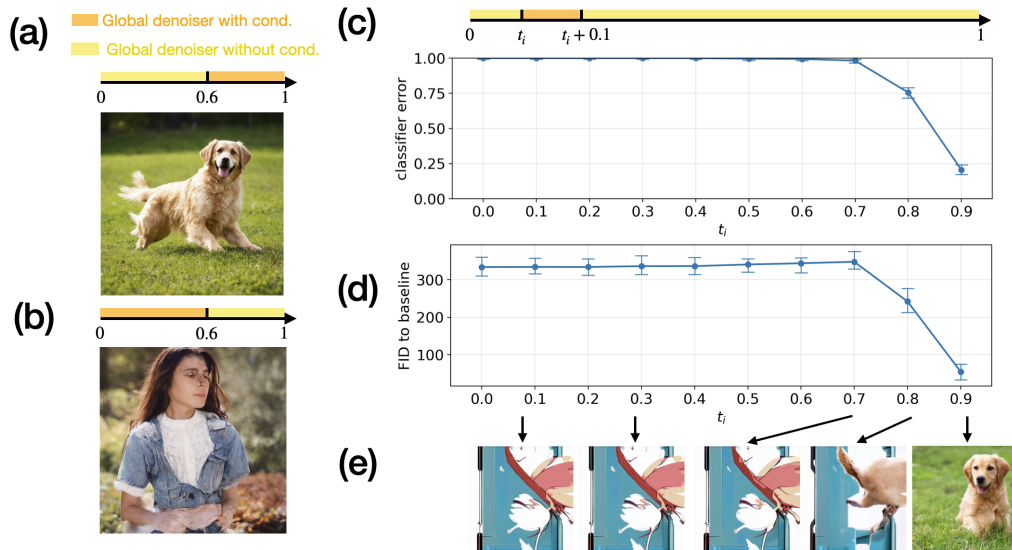


Figure 7: **Windowed conditioning in SD3 medium.** Left column: (a) Golden retriever sample generated with conditioning applied only in the time window  $[0.6, 1.0]$  and no conditioning outside the window. (b) Sample generated with conditioning removed in  $[0.6, 1.0]$  and applied outside the window. Right column: samples generated with conditioning applied only in short windows  $[t_i, t_i + 0.1]$  while scanning  $t_i$ . (c) Classification error as a function of  $t_i$ . (d) FID to always-conditioned samples as a function of  $t_i$ . (e) Visualization of generated samples at different  $t_i$ .

## A Additional Data

Figure 7 and Figure 8 provide the SD3 medium versions of the two windowed sampling experiments discussed in the main text.

One may ask if the score gap plots are typical behaviors for different trajectories. Figure 9 plots the standard deviation of different score gaps due to the randomness in the trajectory. We observe a small fluctuation across all score gaps, indicating that the observed behavior is typical.

We also provide additional data comparing the score gaps along conditional and unconditional sampling trajectories in Figure 10(a-d). For conditional sampling trajectories we report the conditional locality gap since it is relevant to this type of trajectory. Similarly, for unconditional sampling trajectories we report the unconditional locality gap. We observe the same behavior for both types of trajectories. We also compare the conditional and unconditional locality gap for Facebook DiT along the training trajectory. We observe a very small difference.

## B Detailed Review of Earlier Work and Theoretical Background

We give a more detailed review of earlier work and theoretical background in this section.

### B.1 Review of earlier work

Using a diffusion process for generative modeling was proposed by Sohl-Dickstein et al. [2015] and their modern formulations as DDPM and score-SDE were set in Ho et al. [2020] and Song et al. [2021], respectively. Early empirical work, such as Choi et al. [2022] or Meng et al. [2022], already noted that information injection during denoising is not uniform in time, and these observations rapidly inspired a detailed study into dynamics of denoising.

Its origin in non-equilibrium physics invited a study of generative diffusion via a statistical physics lens. Raya and Ambrogioni [2023] found hints of phase transitions in diffusion models, and further

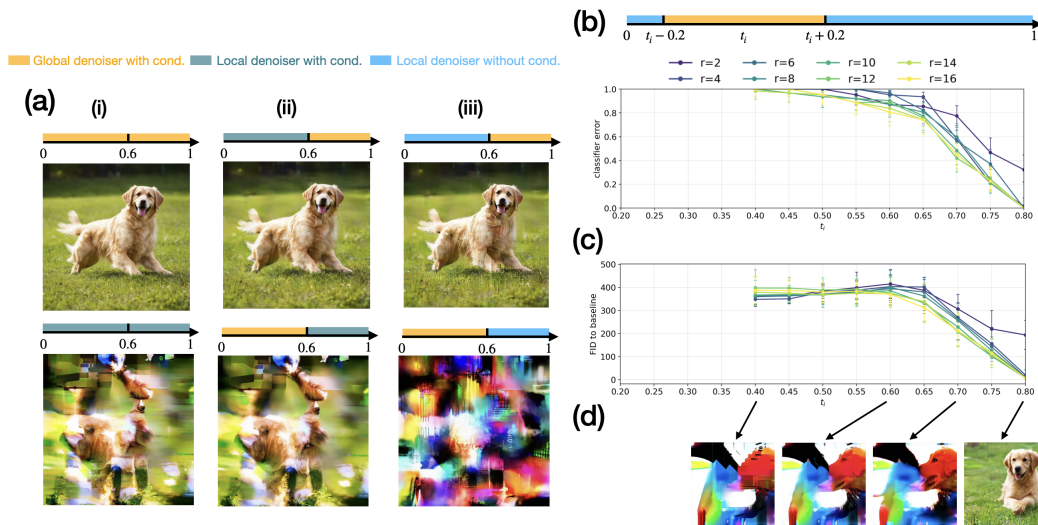


Figure 8: **Windowed local denoising in SD3 medium.** (a) Golden retriever samples generated with different combinations of local and global denoisers. The local denoiser uses radius  $r = 6$ . (i) Top: global denoiser at all times. Bottom: local denoiser at all times. (ii) Top: global denoiser in  $[0.6, 1.0]$  and local conditioned denoiser outside the window. Bottom: local conditioned denoiser in  $[0.6, 1.0]$  and global denoiser outside the window. (iii) Top: global denoiser in  $[0.6, 1.0]$  and local unconditional denoiser outside the window. Bottom: local unconditional denoiser in  $[0.6, 1.0]$  and global denoiser with different  $r$  outside the window. Right column: samples generated with a global denoiser in  $[t_i - 0.2, t_i + 0.2]$  and a local unconditional denoiser outside the window while scanning  $t_i$ . (b) Classification error as a function of  $t_i$ . (c) FID to always-global samples as a function of  $t_i$ . (d) Visualization of generated samples at different  $t_i$  using  $r = 6$ .

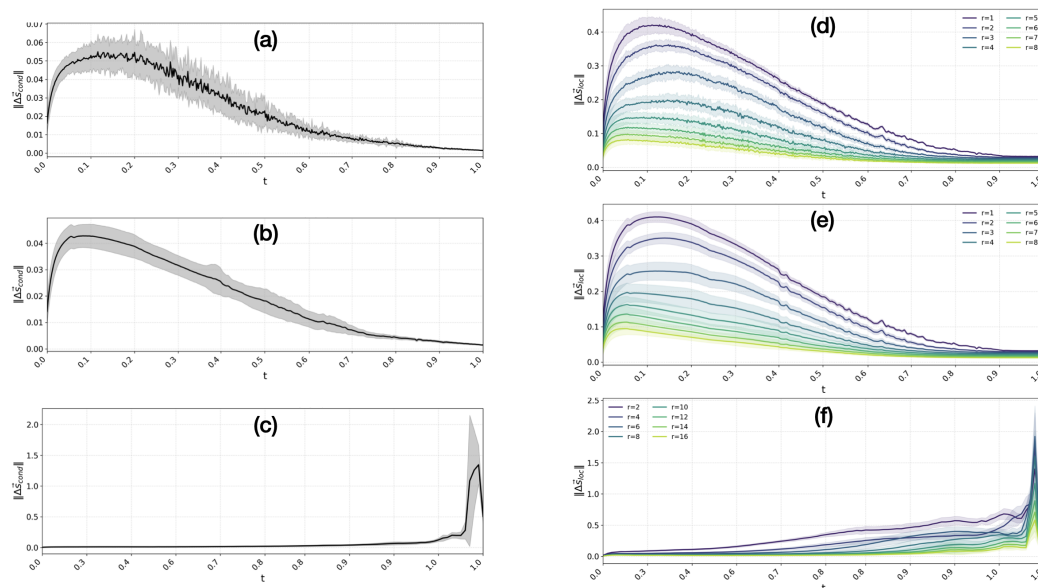


Figure 9: **Fluctuation of score gap.** Plot of score gaps with colored area marking the standard deviation across different trajectories. (a) Conditioning gap and (b) locality for Facenook DiT along the training trajectory. (c) Conditioning gap and (d) locality gap for Facenook DiT along the conditional sampling trajectory. (e) Conditioning gap and (f) locality gap for SD3 medium along the conditional sampling trajectory.

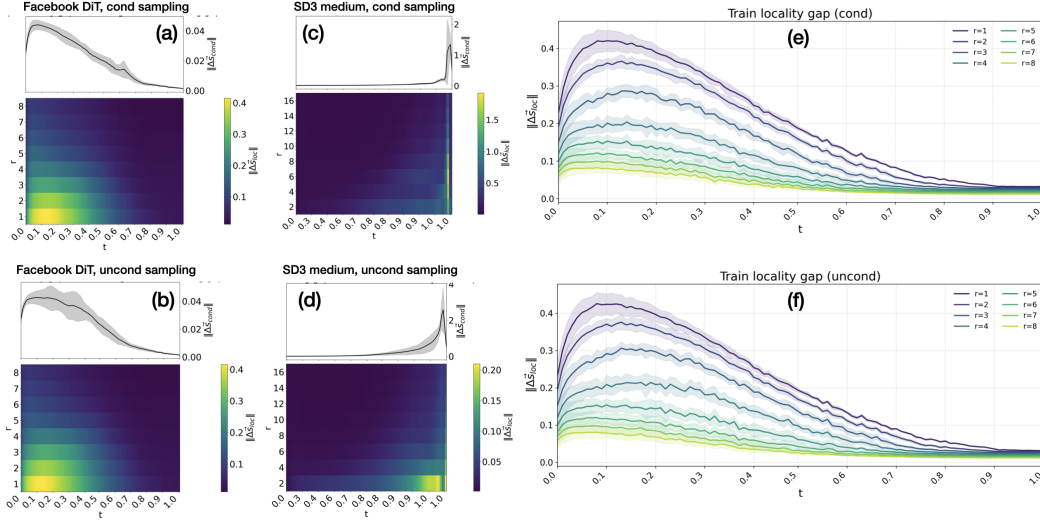


Figure 10: **Score gap along unconditional trajectories.** (a) Conditioning gap (top) and locality gap defined using conditional score function, for Facebook DiT along the conditional sampling trajectory. (b) Conditioning gap (top) and locality gap defined using unconditional score function, for Facebook DiT along the unconditional sampling trajectory. (c) Conditioning gap (top) and locality gap defined using conditional score function, for SD3 medium along the conditional sampling trajectory. (d) Conditioning gap (top) and locality gap defined using unconditional score function, for SD3 medium along the unconditional sampling trajectory. (e,f) Locality gap for Facebook DiT along the training trajectory, for (e) conditional and (f) unconditional score functions. (e,f) are visually indistinguishable because their differences are around 0.01. All colored areas mark the standard deviation across different trajectories.

work by Biroli and Mézard [2023] and Ambrogioni [2025] analyze symmetry breaking (origin of phase transitions) toy models for data distributions. Existence of a phase transition in generation motivates understanding the full denoising process, which was analyzed asymptotically by Biroli et al. [2024], and non-asymptotically by Li and Chen [2024] for when features emerge during generation. Other works by Sclocchi et al. [2025b], Ventura et al. [2026], Yaguchi et al. [2025] studied details of the generation process, such as how various regimes and their time-lengths may be determined the structure of the data itself.

Recent work expands this phase-transition view toward memory, information diagnostics, and control. Pham et al. [2024] study the transition from memorization to generalization through associative-memory spurious states, and Li et al. [2025] develop a broader feature-localization theory for generative models. Handke et al. [2025] measure class-semantic information production along diffusion trajectories, and Stančević and Ambrogioni [2026] connect entropy production, score divergence, and branching dynamics, and Ramachandran et al. [2026] use cross-fluctuations to detect sampling transitions and improve downstream generation and classification. Lu and Tang [2026] study how nonreversible perturbations can steer dynamical regimes by breaking detailed balance. Very recent extensions study entropic signatures of class speciation Handke et al. [2026], out-of-equilibrium pattern formation in trained diffusion models Ambrogioni [2026], and analogous regimes in discrete diffusion models Takahashi et al. [2026]. Our symmetry breaking probe belongs to this lineage, but instead of inferring semantic commitment from generated samples, we directly measure the classifier-free guidance (CFG) score correction  $s_\theta(x_t, t | y) - s_\theta(x_t, t)$  as a model-internal field.

A separate line of work characterizes phases by conditional independence and local recoverability. Given two distributions, Sang and Hsieh [2025] proposed the decay length-scale of conditional mutual information (CMI) (called the ‘Markov length’) as a diagnostic of mixed-state phase transitions, which diverges if the two are in different phases and hence not locally recoverable. Zhang and Gopalakrishnan [2025b] proved that under weak local decoherence, the mixed-state phases are stable, and Yi et al. [2026] proved that finite Markov length is a generic feature of mixed-state phases.

Further work by Zhang and Gopalakrishnan [2025a] proved that the Markov length is finite during diffusion for high-temperature Gibbs states while noting that at low temperature, it may diverge.

Hu et al. [2025] brought this Markov-length perspective directly to diffusion models by defining phases of data distributions analogously to mixed state phases: between two phases, local denoisers fail near a narrow transition window where Markov length diverges, while it remains finite away from this window, which was shown explicitly by calculating the CMI during image generation. Prior work by Hu et al. [2026] has further shown that if a distribution admits a diffusion noise path along which the CMI remains short-ranged, then one can construct a generative procedure that samples from this distribution using only local operations. Conversely, distributions with long-ranged CMI are known to be hard to learn Kumar et al. [2026]. Taken together, these results suggest that the Markov length provides a quantitative indicator of the difficulty of learning and generating a distribution. Our locality-gap heatmaps are an operational analogue of their CMI heatmaps: instead of estimating an information-theoretic decoder, we replace the global denoiser by a local-attention denoiser and directly measure the resulting score and sample degradation. The local-attention intervention itself is related to Swin Transformer by Liu et al. [2021], Neighborhood Attention Transformer by Hassani et al. [2023], neighborhood attention and dilated neighborhood attention by Hassani [2023], Hassani and Shi [2022], DiTFastAttn by Yuan et al. [2024], and Swin DiT by Wu et al. [2025], but our use is diagnostic rather than architectural.

Our contribution is to connect the two phase-transition pictures experimentally. Prior diffusion work asks when semantic decisions, speciation, or collapse occur; prior Markov-length work asks when local neighborhoods suffice for recovery or denoising. We ask whether these two criticalities align in real diffusion transformers by comparing conditioning gaps with locality gaps at the score level and with error-correction and windowed-sampling behavior at the sample level. This also connects to limited-interval guidance by Kynkäänniemi et al. [2024], stage-wise CFG dynamics by Jin et al. [2025], ambient-diffusion studies of memorization by Shah et al. [2025], and latent-hierarchy probing by Sclocchi et al. [2025a].

Understanding locality bias has also been a recurrent topic in literature. Kamb and Ganguli [2024] shows that convolutional diffusion model exploits locality bias explicitly which leads to generalization / creativity. Niedoba et al. [2024] similarly shows the emergence of locality bias in convolutional model and DiT and designs mechanistically interpretable local denoisers to approximate global denoisers. Lukoianov et al. [2025] shows that even for architectures like transformer that are ignorant of locality, they can learn locality structure through data statistics. Intriguingly, while their numerical technique is drastically different, they observe a time window in which model exhibits long-range correlations. This already alludes to the existence of the nonlocality phase transition. Complement to these work, our main contribution is to understand *when* locality bias can be exploited, and how it correlates with symmetry breaking and semantic forcing.

## B.2 Local computation of the score under a Markov property

We provide a more detailed theoretical background about local denoising under approximate Markov property. We encode locality via a rectangular tripartition into the image vector  $X = (x_A, x_B, x_C)$  as shown in Figure 1:  $A$  is the center patch in the black box,  $B$  is the surrounding buffer in gray box, and  $C$  is the rest of the image that we faint out. We would like to understand when local generation of  $A$  is possible, i.e., when the score on region  $A$  can be determined only by the information in  $B$ , without needing to access  $C$ . This is the case if the distribution  $p(x_A, x_B, x_C)$  forms a Markov chain

$$x_A - x_B - x_C, \quad \text{i.e.} \quad p(x_A | x_B, x_C) = p(x_A | x_B), \quad (8)$$

which we call the *Markov property*. Then the score on region  $A$  depends only on  $(x_A, x_B)$ :

$$\begin{aligned} \nabla_{x_A} \log p(x_A, x_B, x_C) &= \nabla_{x_A} \log \left( p(x_A | x_B) p(x_B, x_C) \right) \\ &= \nabla_{x_A} \log p(x_A | x_B). \end{aligned} \quad (9)$$

This motivates a local score approximation to  $s_A(x_A, x_B, x_C)$ , where

$$s_A^{\text{local}}(x_A, x_B) = \nabla_{x_A} \log p(x_A | x_B), \quad (10)$$

which is exact whenever the Markov property holds. We expect the Markov property to hold (at least approximately) in real images. For example, to generate the nose of a dog, the model may only need to look at a local neighborhood containing the snout and eyes, and not the rest of the image.

In practice, the Markov property is only approximate. A standard way to quantify this is the conditional mutual information (CMI)

$$I(A : C | B) = \mathbb{E}_{p(x_A, x_B, x_C)} \left[ \log \frac{p(x_A, x_C | x_B)}{p(x_A | x_B)p(x_C | x_B)} \right]. \quad (11)$$

We define the Markov length  $\xi$  as the length-scale of the empirical decay of CMI with separation: for a neighborhood  $B$  of radius  $r$  around  $A$  and its complement  $C$ , we posit

$$I(A : C | B) \approx I_0 \exp(-d_{AC}/\xi), \quad (12)$$

where  $d_{AC}$  is a distance between regions  $A$  and  $C$  (typically  $d_{AC} = r$  when  $B_r$  is an  $r$ -neighborhood). Intuitively,  $\xi$  is the length scale beyond which information outside the buffer  $B$  is negligible for predicting  $A$ . This was formalised by Hu et al. [2025] as Theorem 1 therein:

**Proposition 1** (Local denoising from finite Markov length). *Consider the  $L_x \times L_y$  image space  $X \in \mathbb{R}^{L_x \cdot L_y}$ . Fix a diffusion time  $t$  and let  $p_t(X)$  denote the noisy image distribution. Suppose the Markov length  $\xi(t) \leq \xi_{\max}$  for all  $t \leq t_c$ . Then a local denoiser with radius  $O(\xi_{\max} \log(L_x L_y / \epsilon))$  that can produce  $p_0(X)$  given  $p_t(X)$  with  $t \leq t_c$ , up to total variation distance of  $\epsilon$ .*

In general, even if the data distribution satisfies the Markov property exactly, the noised distribution  $p_t$  may not, and the Markov length  $\xi(t)$  may vary, perhaps even diverge, as a function of  $t$  Hu et al. [2025]. The divergence of  $\xi(t)$  at some critical time  $t_c$  is understood as a nonlocality phase transition.

Several theory work have characterized how  $\xi(t)$  behaves in discrete spin systems, in both classical and quantum settings. Zhang and Gopalakrishnan [2025a] shows that for high-temperature gibbs state,  $\xi(t)$  remains finite for all  $t$  up to one. This indicates that if a state is in the high-temperature trival thermodynamic phase, then nonlocality phase transition cannot happen during diffusion. At low temperature,  $\xi(t)$  can diverge at some  $t_c$  less than one. In fact, one can prove that it has to if the state exhibit long-range two-point correlations, through a simple light-cone argument. This indicates that nonlocality phase transition can be inevitable in sampling low-temperature distributions. Nevertheless, Zhang and Gopalakrishnan [2025b] proves that  $t_c$  has to be bounded away from zero by a constant amount, indicating that the low-temperature phase is *stable*. Operationally, this implies that a local denoiser should always exist at sufficiently low noise rate.

So far, all existing rigorous results only applies to discrete spin systems and extending the results to continuous systems remains an open challenge. We expect many of the proof technique to break down due to physical reasons, such as the existence of Goldstone mode which challenges stability Mermin and Wagner [1966], and the existence of entropic ordering at high temperature, which challenges the lack of phase transitions Han et al. [2025]. These examples are fine-tuned so we do not expect them to appear in realistic datasets. However, any rigorous results and proof technique would have to be able to rule out these adversarial examples.

## C Details on Experimental Methodology

We provide details about all experiments in this section. All experiment are run on at most a single 80G A100 GPU. Most jobs are run a 1/7 MIG partition of a 80G A100 GPU. All job times are less than a day.

### C.1 Local attention implementations

All local-attention experiments use the same pretrained backbone as the corresponding global baseline and modify only the attention pattern. We replace the attention layer with a radius- $r$  Chebyshev window on the 2D token grid. Queries, keys, and values are projected with the original layer weights; for each image token, the module gathers only keys and values whose grid coordinates satisfy  $\max(|\Delta x|, |\Delta y|) \leq r$ , applies softmax within that window, and reuses the original output projection. For MMDiT joint attention: image-to-image attention is windowed, while text/context tokens remain globally visible so that conditioning is not sparsified.

In practice, this can be implemented directly, or can be implemented by leveraging masking options in existing attention kernels, which gives a significant speedup.

## C.2 Conditioning and Locality Gap

The conditioning and locality gap are defined in the main text. The training trajectory is generated by taking an image from the dataset, and evolving it forward by adding noise. We only compute the training trajectory for Facebook DiT since its training dataset is ImageNet which is publicly accessible Deng et al. [2009]. Also note that there is no distinction between conditional and unconditional training trajectory. The sampling trajectory is generated by starting from complete noise and evolving it backward using the diffusion model. Sampling trajectory can be either conditional or unconditional. We also note that all score gaps and their  $l_2$  norms are directly computed in the latent space. We observe that score gaps in latent space translates to a larger gap in the pixel space when  $t$  is closer to zero. This tilts the score gap plot towards the beginning. We hypothesize that this enhanced sensitivity is due to the formation of data manifold near clean image which could enhance perturbation in the latent space. We report the  $l_2$  norm divided by the number of image tokens.

For Facebook DiT-XL results presented in Figure 3, we take 500 steps along the training and sampling trajectory. We take 20 samples at each time step. We use the HuggingFace diffusers implementation of DPMSolverMultistepScheduler Lu et al. [2022, 2025]. We evaluate 20 samples for each time step. Image size is fixed to  $256 \times 256$  by the model. For conditioning, we use class 207 (golden retriever). We do not observe qualitative differences between different class labels.

For SD3 medium, we take 100 steps along the sampling trajectory. We take 10 samples at each time step. We use the StableDiffusion3Pipeline from HuggingFace diffusers. We use an image size of  $512 \times 512$ . We use a CFG strength of 4.0 in both cases. For conditioning, we use prompt “a golden retriever playing in a park, high detail, soft lighting”. Again, we do not observe qualitative differences between differnt prompts.

For both models, the VAE has a eight-to-one compression ratio, and they both organize a two-by-two latent patch into a token. Therefore, both model have a token patch size of  $16 \times 16$  in the pixel space. This means that for Facebook DiT-XL, setting  $r = 16$  reduces local attention to global dense attention. For SD3 medium in our setup, this  $r$  becomes 32.

Subsequent experiments inherit the same setup unless otherwise noted.

## C.3 Forward-backward experiments

For Facebook DiT, we use 20 clean-generation steps, 50 denoising steps, and evaluate at 40 linearly spaced noise levels with  $t_{\text{norm}} \in [0.1, 1.0]$ . For each noise level, the experiment draws 40 independent noise realizations.

For both models, We use microsoft/resnet-50 for classification He et al. [2016], Hugging Face and Microsoft [2025]. We report the standard deviation of the classifier error which is analytically determined from the Bernoulli distribution, since classification is either correct or incorrect. For a datapoint with classification error  $p$  and with  $n$  samples, the one-sigma error is given by  $\sqrt{p(1-p)/n}$ .

## C.4 Conditioning window and locality window experiments

We use 40 sampling steps for all window experiments. For conditioning window experiments for both models, we use a window size of 0.1 and scan  $t_i$  from 0 to 0.9 by steps of 0.1 (setting  $t_i > 0.9$  truncates the window size). We use 500 samples per  $t_i$ . For locality window experiments for Facebook DiT, we use a window size of 0.4 and scan  $t_i$  from 0.2 to 0.8 by steps of 0.05 (setting  $t_i > 0.9$  or  $t_i < 0.2$  truncates the window size). We use 500 samples per  $t_i$ . For SD3, we start  $t_i$  at 0.4 and use 62 samples per  $t_i$  to reduce compute.

Our FID follows from the standard definition Heusel et al. [2017]. We use the pool3 layer of the inception V3 network Szegedy et al. [2016] as features in computing the Gaussian Fréchet distance. Note that we are in a sample-deficient regime which will lead to significant overestimate of FID. This is fine since we are not concerned about the absolute value of FID, but at which  $t_i$  it becomes the smallest. We compute the one-sigma error by bootstrap resampling.

## D Limitation of Our Work

Our empirical study is currently limited to two representative diffusion transformer systems: a class-conditional ImageNet DiT and a text-conditioned MMDiT/SD3 model. Although these models cover two common conditioning mechanisms and show consistent concurrence between the symmetry-breaking and nonlocality critical windows, a broader evaluation across architectures, model scales, datasets, samplers, and prompt distributions is needed before claiming universality. In addition, our truncated-attention DiT should be understood as an approximate local denoiser rather than a strictly local one, where information can still propagate across distant patches through multiple layers of local attention. Constructing a numerically faithful strictly local score estimator for modern pretrained diffusion models is itself challenging; future work could test whether the same concurrence persists under more diverse architectures and under stricter or independently trained local denoisers.

Our conclusions are also empirical rather than theoretical. The observed concurrence is supported by score-gap measurements and windowed sampling interventions, but we have not proven that symmetry-breaking and nonlocality transitions must coincide in general. Moreover, our analysis has not yet systematically compared how the identified critical windows in the latent space. Some quantitative estimates, especially FID and sliding-window results, are based on finite samples and should be interpreted as evidence for relative timing rather than precise estimates of the phase transition window. Developing sharper statistical tests and a theory connecting these operational probes to Markov length or conditional mutual information remains an important direction for future work.

We are also not able to quantify the width of the critical window. We expect that different definitions give rise to different width. Only in well-defined “thermodynamic limit” can one give a unified definition (and critical window can also collapse to a critical point in this limit). Ideally, it would be useful to understand the criticality better by probing certain universal scaling behavior as in statistical mechanics. However, it is currently unclear what is the correct scaling variable and scaling hypothesis that captures the behavior of diffusion models. We leave such a scaling analysis to future work.